Fréedericksz transitions in supra-μm nematic droplets

S. Kralj
J. Stefan Institute, University of Ljubljana, Jamova 39, 61000 Ljubljana, Slovenia

S. Žumer
Physics Department, University of Ljubljana, Jadranska 19, 61000 Ljubljana, Slovenia
and Liquid Crystal Institute, Kent State University, Kent, Ohio 44242

(Received 19 July 1991)

The stability of uniaxial nematic-liquid-crystalline structures in supra-μm-size spherical cavities that impose a weak homeotropic anchoring is studied theoretically. The equilibrium equations are obtained with the minimization of the deformation, surface, and field contributions to the free energy and are solved numerically. The dependencies of the solutions on the ratio of elastic constants K_{33}/K_{11}, K_{24}/K_{11}, anchoring strength, and external field strength are discussed, and the stability diagrams with lines of structural (Fréedericksz) transitions are constructed. In the region of strong anchoring and large external field strengths, a triple point, where radial, nonsingular axial, and axial structure with the line defect, is predicted. Particular attention is paid to the inversion point corresponding to the critical-field strength above which radial structure is no longer stable. Two possible methods for saddle-splay elastic constant K_{24} determination are suggested.

PACS number(s): 61.30.Gd, 64.70.Md, 61.30.Jf

I. INTRODUCTION

Surface-induced phenomena in liquid-crystal samples with microscopically restricted geometry are the matter of recent particular interest. Nematic-liquid-crystal droplets dispersed in a solid polymer [1–4] are typical examples of such systems where relatively high surface-to-volume ratios are easily reached. These polymer dispersed liquid crystal (PDLC) materials are obtained by a polymerization-induced phase separation with average droplet radius ranging from less than 0.1 μm to more than 10^2 μm, depending on the preparation procedure. The spatial dependence of nematic ordering within droplets depends on the relative strength of elastic forces, external fields, and surface interactions. The confined phase can be either [5,6] isotropic, paranematic, isotropic with a boundary nematic layer, or nematic. These phases can exhibit a variety of nematic director fields (configurations). The best known are bipolar and concentric structures for tangential [7–10] anchoring and radial and axial structures for homeotropic [8,9,11] anchoring. For materials with small twist elastic constants, a reduction of the splay elastic free energy leads to twisted structures [12,13]. In droplets where anchoring is neither homeotropic nor tangential, structures with lower symmetry appear. More defects and features of the both radial and axial structures have been observed [9]. Some of these structures in supra-μm droplets dispersed in a liquid or solid have been studied using optical microscopy [8–12]. Much less is known about cholesteric droplets where best known is the structure with a radial defect occurring in the case of tangential anchoring [14]. More indirect studies such as light attenuation [15] and deuterium NMR [16–18] have been used for sub-μm nematic droplets.

The transitions between various stable structures are kinds of Fréedericksz transitions [19]. In contrast to the field-induced transitions in planar systems, the transitions are of first order. To find conditions where transitions occur, model structures for nematic droplets must be obtained. One usually starts with a minimization of a phenomenological expression for the free energy. Depending on the droplet size two approximate approaches can be used: the Frank-Oseen approach [20] for supra-μm droplets where nematic free energy density is expanded in terms of the derivatives of the components of the nematic director $\mathbf{n}$, and the Landau–de Gennes approach [19] for sub-μm droplets where the free-energy density is expanded in terms of a nematic order parameter and its derivatives. In both cases the minimum number of terms having the required symmetry are considered. Recently, particular attention has been paid to surface (saddle-splay and splay-bend) terms that are usually neglected [19,21].

In this paper we study stability of phases in supra-μm nematic droplets where a weak homeotropic anchoring is enforced on its spherical surface. In Sec. II we start with the most general Landau–de Gennes expansion of the free energy and then introduce approximations that yield a Frank-type free energy. This allows us to write the well-known Frank elastic constants in terms of the Landau–de Gennes expansion coefficients and to avoid nonphysical choices for elastic constants in our model. The elastic free energy, which includes the surface saddle-splay term in addition to the bulk terms, is minimized together with external field and interfacial contribution. We limit our discussion to nontwisted cases (i.e., with relatively large K_{22}). In Sec. III solutions with radial, deformed radial, and axial (with and without line defect) director fields are presented. The lines of structural transitions in the phase stability diagram are obtained. The theoretical results and the available experimental

data are discussed in Sec. IV. In Sec. IV we also discuss how K_{24} can be extracted from an experimentally determined stability diagram.

II. FREE ENERGY

To determine the stable structure of a chosen system at constant volume and temperature, the minimization of the free energy is usually used. We start with a general Landau–de Gennes–type expansion [19,22–24] of the free-energy density in terms of the tensor order parameter Q_{ij} [22]. The density can be divided in homogeneous, inhomogeneous, surface, and field parts,

$$f(\mathbf{r})=f_h(\mathbf{r})+f_e(\mathbf{r})+f_s(\mathbf{r})+f_f(\mathbf{r}) , \tag{1}$$

where

$$f_h(\mathbf{r})=f_0(T)+\frac{a}{2}(T-T_*)Q_{ij}Q_{ji}-\frac{b}{3}Q_{ij}Q_{jk}Q_{ki} +\frac{c_1}{4}(Q_{ij}Q_{ji})^2+\frac{c_2}{4}Q_{ij}Q_{jk}Q_{kl}Q_{li}+\cdots \tag{2}$$

is the homogeneous [24] part of the free energy density with $a(T-T_*)$, b, c_1, and c_2 the expansion coefficients. T_* is the temperature of the supercooling limit. Indices $i,j,l,k,\ldots$ stand for any of our three orthogonal coordinate axes. The standard notation, where a double appearance of any index in each term stands for the summation over that index, is used,

$$\begin{aligned} f_d(\mathbf{r})=&L_1^{(2)}Q_{jk,i}Q_{jk,i}+L_2^{(2)}Q_{ij,i}Q_{kj,k}+L_3^{(2)}Q_{jk,i}Q_{ik,j}+L_5^{(2)}Q_{ik,ij}Q_{jk}+L_6^{(2)}Q_{jk,ii}Q_{jk} \\ &+L_1^{(3)}Q_{ij}Q_{ij,k}Q_{kl,l}+L_2^{(3)}Q_{ij}Q_{ik,j}Q_{kl,l}+L_3^{(3)}Q_{ij}Q_{ik,k}Q_{jl,l} \\ &+L_4^{(3)}Q_{ij}Q_{ik,l}Q_{jk,l}+L_5^{(3)}Q_{ij}Q_{ik,l}Q_{jl,k}+L_6^{(3)}Q_{ij}Q_{ik,l}Q_{kl,j}+\cdots \end{aligned} \tag{3}$$

is the inhomogeneous [22,23] part of the free-energy density associated with the nonuniform ordering. The expansion coefficients $L_i^{(j)}$ are temperature-independent generalized elastic constants. $Q_{ij,l}$ denotes the partial derivation of Q_{ij} with respect to the lth coordinate. To describe the chiral nematic phase the term

$$L_4^{(2)}\epsilon_{ijk}Q_{il}Q_{jl,k} , \tag{4a}$$

with ϵ_{ijk} as the Levi-Cevita antisymmetric tensor with properties

$$\epsilon_{ijk}=\begin{cases} 1, & ijk=123,231,312 \\ -1, & ijk=213,321,132 \\ 0, & \text{elsewhere} \end{cases} \tag{4b}$$

must be added to Eq. (3).

For the interaction of the liquid crystal with the surrounding medium [25,26] we assume a contact nature of the interaction described by a δ function and a linear dependence on the order parameter [5,25]

$$f_s=-\frac{w_0}{3}e_iQ_{ij}e_j\delta(R-r) . \tag{5}$$

Here e_i are the components of the unit vector along the preferred surface anchoring direction and w_0 measures the strength of the interfacial interaction. Usually w_0 multiplied by the nematic-order parameter S is defined as the anchoring strength denoted by W_0 [26]. In a more detailed discussion the terms with higher powers of Q should be taken into account [27].

The external field contribution will be explicitly written only for the magnetic case

$$f_f=-\frac{\mu_0}{2}H_i\chi_{ij}H_j , \tag{6}$$

where $\mathbf{H}$ is the magnetic field and χ_{ij} the magnetic susceptibility tensor related to the order parameter [28]

$$\chi_{ij}=\chi\delta_{ij}+\tfrac{2}{3}\Delta\chi Q_{ij} . \tag{7}$$

$\Delta\chi$ is the difference between the principal values corresponding to the directions parallel and perpendicular to $\mathbf{n}$; χ is the isotropic part of the susceptibility. It should be stressed that the effect of the electric field could be treated in a similar way, but in comparison to the magnetic field case it substantially varies over the droplet. This is a consequence of a large spatial variation of the dielectric constant in such an inhomogeneous structure, while in the magnetic case χ is small throughout. The internal electric field also can be significantly affected by the electric conductivity of the liquid crystal and the surrounding medium. Therefore in most cases a complete solution of the electric case must include a simultaneous minimization of the free energy and solving the corresponding Maxwell equations.

Here we treat supra-μm droplets far below the nematic-isotropic phase transitions, where effects of local biaxial ordering and of spatial dependence of the orientational order are negligible. The ordering will therefore be described by the nematic director field $\mathbf{n}(\mathbf{r})$ and by a spatially independent scalar nematic-order parameter [24] $S=\frac{1}{2}\langle 3\cos^2\theta_m-1\rangle$, where $\langle\ \rangle$ stands for the statistical average over angles between the director and molecular axis. The tensor order parameter thus reduces to

$$Q_{ij}(\mathbf{r})=\frac{S}{2}[3n_i(\mathbf{r})n_j(\mathbf{r})-\delta_{ij}] . \tag{8}$$

Further we limit our discussion to the normal anchoring ($\mathbf{e}=\mathbf{e}_r=\mathbf{r}/r$) and after some rearrangements write Eq. (1) in the following form:

$$f/(K_1/R^2)=\tfrac{1}{2}((\nabla\cdot\mathbf{n})^2+k_{22}(\mathbf{n}\cdot\nabla\times\mathbf{n})^2+k_{33}(\mathbf{n}\times\nabla\times\mathbf{n})^2-k_{24}\{\nabla\cdot[\mathbf{n}(\nabla\cdot\mathbf{n})+\mathbf{n}\times\nabla\times\mathbf{n}]\})$$
$$+k_{13}\nabla\cdot[\mathbf{n}(\nabla\cdot\mathbf{n})]+[1-(\mathbf{n}\cdot\mathbf{e}_r)^2]\frac{\mu}{2}\delta(1-\rho)-\tfrac{1}{2}h^2(\mathbf{e}_H\cdot\mathbf{n})^2+f_h' \ , \tag{9}$$

where f_h' represents all homogeneous (temperature- and field-dependent) terms, $\rho=\mathbf{r}/R$ is a dimensionless position vector where ∇ is the gradient operator in ρ space, $\mathbf{e}_H=\mathbf{H}/H$ is a unit vector, and $h=R/\xi$ with

$$\xi^{-1}=\sqrt{H^2\mu_0\Delta\chi S/K_{11}} \tag{10a}$$

as the correlation length measuring the distance over which the ordering (introduced by a surface) persists in the field [28]. Further the dimensionless parameters $\mu=R/d$ with

$$d=\frac{K_{11}}{W_0}=\frac{K_{11}}{w_0 S} \tag{10b}$$

as the extrapolation length [24] and $k_{ij}=K_{ij}/K_{11}$ with K_{ij} as the Frank elastic constants of the system given by

$$K_{11}=\frac{9S^2}{2}(2L_1^{(2)}+L_2^{(2)}+L_3^{(2)}-L_5^{(2)}-2L_6^{(2)})$$
$$+\tfrac{9}{4}S^3(-L_2^{(3)}+2L_3^{(3)}+L_4^{(3)}+2L_5^{(3)}-L_6^{(3)}) \ , \tag{11a}$$

$$K_{22}=9S^2(L_1^{(2)}-L_6^{(2)})+\frac{9S^3}{4}L_4^{(3)} \ , \tag{11b}$$

$$K_{33}=\frac{9S^2}{2}(2L_1^{(2)}+L_2^{(2)}+L_3^{(2)}-L_5^{(2)}-2L_6^{(2)})$$
$$+\frac{9S^3}{4}(2L_2^{(3)}-L_3^{(3)}+L_4^{(3)}-L_5^{(3)}+2L_6^{(3)}) \ , \tag{11c}$$

$$K_{24}=\frac{9S^2}{2}(2L_1^{(2)}+L_3^{(2)}-\tfrac{1}{3}L_5^{(2)}-2L_6^{(2)})$$
$$+\frac{9S^3}{2}(L_4^{(3)}+2L_5^{(3)}-L_6^{(3)}) \ , \tag{11d}$$

$$K_{13}=\frac{S^2}{4}L_5^{(2)} \ . \tag{11e}$$

K_{11} is the elastic constant for the splay, K_{22} for the twist, and K_{33} for the bend deformation. All three types of deformations contribute to the bulk elastic free energy. K_{24} saddle-splay and K_{13} splay-bend elastic constants correspond to the deformations that contribute to the surface elastic free energy.

In a single elastic constant approximation, where only the constant $L_1^{(2)}$ associated with pure quadratic terms is nonzero, we have $K_{11}=K_{22}=K_{33}=K_{24}=9S^2L_1^{(2)}$ and $K_{13}=0$. Taking into account constants associated with other second-order terms, one finds $K_{11}=K_{33}\neq K_{22}\neq K_{24}$ and $K_{13}=0$, where all nonzero constants are of the same order of magnitude. Including terms with second derivative one also finds $K_{13}\neq 0$ and further including third-order terms $K_{11}\neq K_{33}$. In most nematic-liquid crystals [29], $K_{33}>K_{11}>K_{22}$ is realized. While there is no information about K_{13} [30,31], preliminary data about K_{24} have been recently published [21,32–34]. It should be mentioned that from the Maier-Saupe molecular approach a different equation relating K_{24} and K_{ii} is obtained, namely [35]

$$K_{24}=\tfrac{1}{2}(K_{11}+K_{22}) \ . \tag{11f}$$

Here it should be stressed that we follow the notation of Saupe used in his 1982 paper [36] where the originally used sum $K_{24}+K_{22}$ (Frank [20], Nehring and Saupe [35]) is substituted by $K_{24}/2$. Further it is worthwhile to mention the equivalency of different forms of the saddle-splay term. $\nabla\cdot[\mathbf{n}(\nabla\cdot\mathbf{n})+\mathbf{n}\times\nabla\times\mathbf{n}]=\nabla\cdot[\mathbf{n}(\nabla\cdot\mathbf{n})-(\mathbf{n}\cdot\nabla)\mathbf{n}]$ $=(\nabla\cdot\mathbf{n})+(\nabla\times\mathbf{n})-\nabla\mathbf{n}:\nabla\mathbf{n}=n_{i,i}n_{j,j}-n_{i,j}n_{j,i}$ (where according to the standard notation the second index stands for the corresponding derivative and the summation must be carried over all repeated indices).

Recent papers also claim [30,31] that no continuous solution of the equilibrium equations is possible at the nematic-liquid-crystal boundary in the case of a finite K_{13} value unless bulk terms including second derivatives of the elastic free energy are taken into account. Because nothing is known about the corresponding elastic constants we will consider that $K_{13}=0$.

The minimization of the total free energy $F=\int f(\mathbf{r})d\mathbf{r}$ leads to Euler-Lagrange differential equations (see appendix). We limit our discussion to cases without twist deformations ($K_{22}>K_{11}$ limit) so that the nematic director can be expressed in spherical coordinate system as

$$\mathbf{n}=-\sin\theta\mathbf{e}_\vartheta+\cos\theta\mathbf{e}_r \ , \tag{12}$$

where $\mathbf{e}_r$ and $\mathbf{e}_\vartheta$ are unit vectors of the spherical coordinate system and θ the angle between $\mathbf{e}_r$ and $\mathbf{n}$. The vector field $\mathbf{n}$ is, in this case, completely described by a scalar field $\theta(r,\vartheta)$. Using differential equations written in the Appendix one can easily show that θ satisfies the differential equation

$$(\sin^2\theta+k_{33}\cos^2\theta)\left[\frac{\partial^2\theta}{\partial\rho^2}\rho^2+2\frac{\partial\theta}{\partial\rho}\rho\right]+(\cos^2\theta+k_{33}\sin^2\theta)\left[\frac{\partial^2\theta}{\partial\vartheta^2}+\frac{\partial\theta}{\partial\vartheta}\cot\vartheta\right]-\frac{\sin 2\theta}{2}(\cot^2\vartheta-1)$$
$$-(1+k_{33})\cot\vartheta\sin^2\theta+\frac{(1-k_{33})}{2}\left\{\sin 2\theta\left[\rho^2\left[\frac{\partial\theta}{\partial\rho}\right]^2+\rho\frac{\partial\theta}{\partial\rho}\cot\vartheta-\left[\frac{\partial\theta}{\partial\vartheta}\right]^2+\frac{\partial\theta}{\partial\vartheta}+2\rho\frac{\partial^2\theta}{\partial\rho\partial\vartheta}\right]\right.$$
$$\left.+2\cos 2\theta\frac{\partial\theta\partial\theta}{\partial\vartheta\partial\rho}\rho\right\}-h^2\rho^2\frac{\sin[2(\theta-\vartheta)]}{2}=0 \tag{13}$$

in the droplet and the differential equation

$$\frac{\partial\theta}{\partial\rho}(\sin^2\theta+k_{33}\cos^2\theta)+\frac{\partial\theta}{\partial\vartheta}(1-k_{33})\sin\theta\cos\theta-\cos\theta\sin\theta(2-k_{33})+\cot\vartheta\sin^2\theta+\mu\cos\theta\sin\theta+k_{24}(\sin2\theta-\cot\vartheta\sin^2\theta)=0 \tag{14}$$

on its surface.

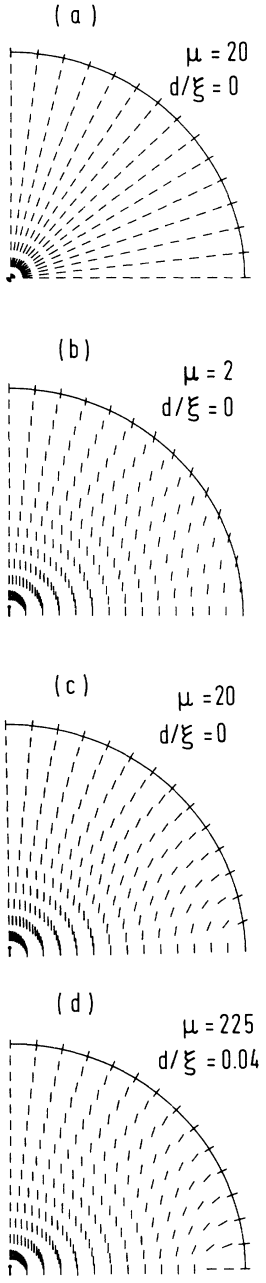

FIG. 1. Director fields in spherical nematic droplets with homeotropic anchoring on the surface are shown for several values of the anchoring strength parameter μ and external field strengths parameter d/ξ: (a) radial structure in zero field; (b) zero field axial structure for small anchoring parameter; (c) zero field axial structure for intermediate anchoring parameter close to the axial-radial transition point; (d) axial structure with defect line close to the triple point. Director fields are obtained numerically for the case $K_{11}=K_{33}$, $K_{24}=K_{13}=0$.

III. STABLE STRUCTURES

Solving the above equations by using the overrelaxation method [6], radial and axial solutions satisfying the homeotropic boundary conditions are found. In the radial structure the nematic director has, at least in weak fields [Fig. 1(a)], predominantly radial direction with a point defect in the center of the droplet. In the axial structures [Figs. 1(b)–1(d)] the director field is predominantly axial in the central region, but close to the surface it tends to be normal to the surface particularly in strong anchoring cases. In these structures the largest deformation is localized close to the droplet equator. While in the weakly anchored case there are no defects in the axial structures; at stronger anchoring strengths the equatorial deformation [Fig. 1(d)] increases, and the axial structure with a disclination line with the defect strength $\frac{1}{2}$ [28] may be stable. This structure has a line defect in the equatorial plane shifted towards the droplet interior so that the nematic director field is on the droplet surface almost everywhere perpendicular to it.

In the following we study the dependence of the stability of the above structures on the anchoring strength, droplet radius, ratio of elastic constants K_{33}/K_{11}, and the external field strength. The stability regions are simply determined by comparing numerically evaluated free energies F_i ($i=r$: radial structure; $i=a$: axial structure without a defect; $i=d$: axial structure with the line defect).

Let us first study the dependence of the free energy of

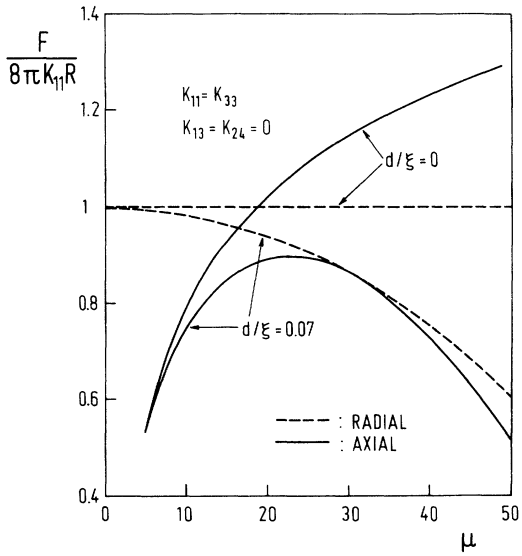

FIG. 2. Free-energy dependencies of the axial and radial structures on the anchoring strength parameter μ are shown for different values of the external field.

the radial and axial structure in the approximation of equal bulk elastic constants ($K_{33}=K_{11}=K_{22}$), neglecting the saddle-splay contribution ($K_{24}=0$). In Fig. 2 the free energies of both structures are shown as functions of the dimensionless parameter μ at $d/\xi=0$ and $d/\xi=0.07$. The parameter $\mu=RW_0/K_{11}$ measures the relative anchoring strength and the parameter $d/\xi=H\sqrt{\mu_0\Delta\chi K_{11}}/S/w_0$ the relative external field strength. At small values of μ ($\mu<10$) the director field is mostly influenced by elastic forces and external fields. Therefore a nonsingular axial nearly homogeneously oriented structure is stable [see Fig. 1(b)] for all values of the external field. With increasing anchoring strength parameter μ, the axial configuration departs further and further from a homogeneously oriented nematic phase [Figs. 1(b) and 1(c)] and its free energy becomes comparable to the free energy of the radial structure. If the field strength parameter is below a limiting value (in our case $d/\xi<0.07$) and the anchoring strength parameter μ is above a limiting value (in our case ~ 18 for $\xi=0$ and ~ 29 for $\xi=0.07$) the radial structure is stable. At finite value of the external field the range of the stable axial structure can be reentered by increasing the parameter μ. This is a result of relatively higher deformation free energies in strongly anchored radial structures as compared to the corresponding axial cases. In Fig. 3 the dependence of the free energy of a droplet on the external field strength is presented for a constant anchoring strength that is chosen strong enough to enable the stability of radial structures at low external field strengths. It is demonstrated that with increasing the field parameter d/ξ, a discontinuous transition point is reached where the axial structure becomes stable.

With increasing anchoring strength ($\mu\gg 200$) the localization of the deformation at the equator [compare Figs. 1(b)–1(d)] becomes more pronounced, above $\mu\sim 240$ in the presence of an external field with the relative strength $d/\xi\sim 0.03$ the axial structure with a line defect in the equatorial plane becomes the most stable [Fig. 1(d)]. The contribution of the defect region was evaluated approximately by introducing an isotropic core. Its radius was estimated from a simple condition that the free-energy density of a deformed nematic phase cannot be higher than the free-energy density of the isotropic phase. In our case core radius was about 4 nm. The estimated error in evaluating F_d is approximately 10%, while the free energies of the radial and nonsingular axial structures are accurate within 1%. In Fig. 4 the

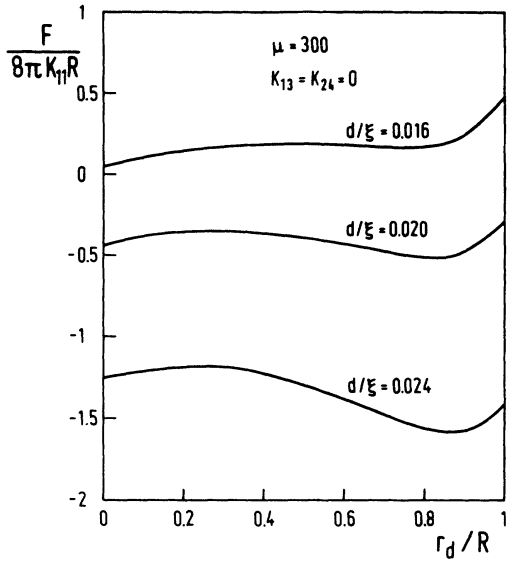

FIG. 4. Dependence of the free energy of the axial structure with defect as a function of the distance of the line defect from the droplet center for different values of the external field.

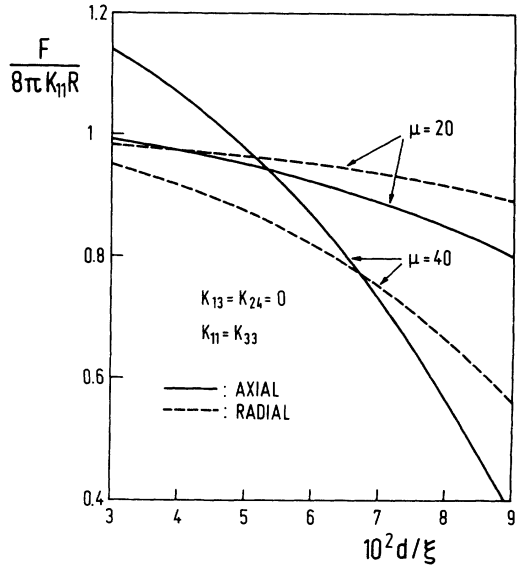

FIG. 3. Dependencies of the free energy of axial and radial structures on the external field strength for two values of the relative anchoring strength parameter μ.

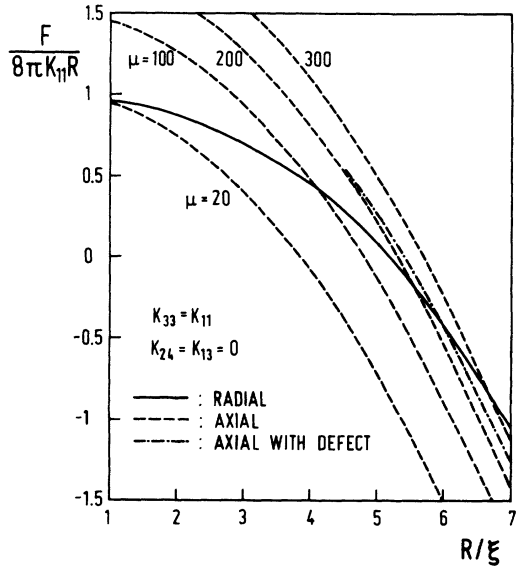

FIG. 5. Comparison of the free-energy dependencies on the ratio R/ξ for different μ values.

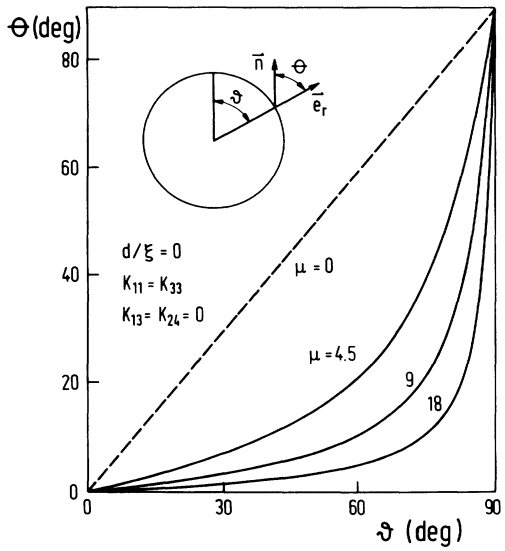

FIG. 6. Orientation of the director field on the droplet surface for different μ values. The dotted line shows the angle θ for a perfectly homogeneous nematic structure.

dependence of the free energy on the relative distance of the line defect from the droplet center r_d/R is shown for this structure in several external field strengths at the constant relative anchoring strength $\mu \sim 300$. At low field values the radial structure with the defect in the droplet center is stable. With increasing field strength at $d/\xi \sim 0.016$ a local minimum in F_d appears at $r_d/R \sim 0.75$, corresponding to the ratio $R/\xi \sim 4.5$. This minimum corresponds to the metastable axial structure with a defect line. At the critical external field strength where the structure with a line defect becomes more stable than the radial one, a first-order structural transition occurs. Keeping $\mu = 300$ and increasing the field further, the position of the line defect r_d/R changes from

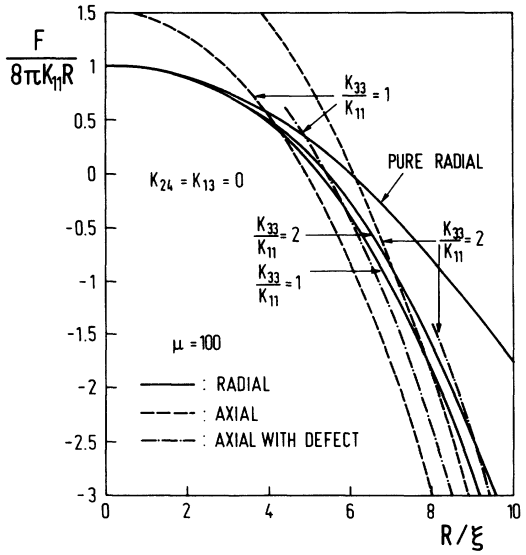

FIG. 7. Comparison of the free-energy dependencies on the parameter R/ξ for different ratios of elastic constants.

0.75 to 0.9 until at $d/\xi \sim 0.045$; the axial structure with a defect line discontinuously transforms into the usual axial structure.

In the case of strong anchoring and in the approximation of equal elastic constants, the solution of Euler-Lagrange equations depends only on the ratio R/ξ [see Eq. (13) for the case $K_{33} = K_{11}$]. In Fig. 5 the free energy of structures depending on R/ξ is shown for different μ values for the case of equal elastic constants. Calculated values of the free energy of the radial structure for

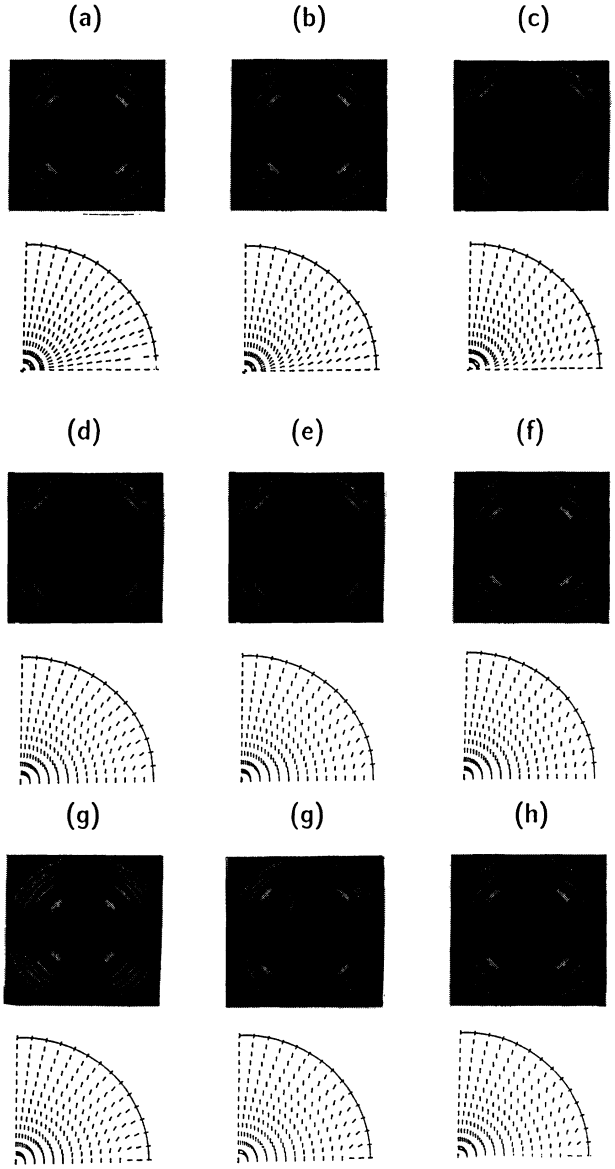

FIG. 8. Simulated monochromatic light polarization microscope textures and the corresponding director fields for different values of the field strength parameter d/ξ at $\mu = 250$: (a) radial, $d/\xi = 0.02$; (b) radial, $d/\xi = 0.04$; (c) radial, $d/\xi = 0.06$; (d) axial, $d/\xi = 0.02$; (e) axial, $d/\xi = 0.04$; (f) axial, $d/\xi = 0.06$; (g) axial with defect, $d/\xi = 0.02$; (h) axial with defect, $d/\xi = 0.04$; (i) axial with defect, $d/\xi = 0.06$. Simulation [37] was performed for $R/\lambda = 28$ and with the extraordinary index of refraction $n_{\parallel} = 1.7$ and the ordinary index of refraction $n_{\perp} = 1.5$.

different μ values lie on the same curve, which indicates that the approximation of strong anchoring for this structure is valid in the whole regime studied. For the axial structure with a defect line the variation of the free energy with μ is within numerical error; therefore its dependence on R/ξ is also represented by a single curve. The dependence of the axial free energy on μ at a fixed R/ξ value indicates changes in the director field even in the region where the anchoring is very strong. Figure 6 shows the behavior of $(\theta)_{\text{surface}}$, the average orientation angle of nematic molecules at the droplet surface in zero field ($d/\xi=0$) for different anchoring strengths. It is evident that except close to the equator the surface angle of the director is already stabilized in the neighborhood of the transition into the radial structure ($\mu\sim 18$). The dotted line indicates the case for parallel orientation of molecules, realized at $\mu \ll 1$ or $d/\xi \gg 1$.

The influence of the ratio of elastic constants K_{33}/K_{11} on the stability of different structures is shown in Fig. 7, where free energies of structures are presented as functions of R/ξ for different ratios of K_{33}/K_{11}. The free energy of the undeformed radial structure, where only splay deformation is present, does not depend on the value of the K_{33} constant. In higher external fields ($R/\xi > 3$) molecules in the radial structure partially orient in the field direction, and the free energy becomes K_{33} dependent. The free energy of the axial structure, since it includes more bend deformation, is more influenced by the magnitude of K_{33} than a deformed radial structure. The axial structure with the line defect [Fig. 1(f)] near the droplet surface is similar to the radial structure and has no bend deformation, while in the droplet interior it is similar to the usual axial structure [Fig. 1(d)]. For this reason, the behavior of F_d is somewhere in between that of F_a and F_r.

The structure studies of supra-μm droplets can be made with a polarizing optical microscope. To show how such microscope textures would look we have used a recently developed method for texture simulations in nematic droplets [37]. One must be aware that this method where diffraction, refraction, and reflection are neglected and only phase shifts of ordinary and extraordinary rays are taken into account can be used only in the case of supra-μm droplets with small differences in indices of refraction. Figure 8 shows director fields and simulated textures of both the radial and axial structures (with the line defect and without it) for different external field strengths at the constant anchoring strength parameter $\mu=250$. One sees that brushes of the radial and axial structures substantially differ, while differences between a nonsingular axial structure and the one with the defect line are much more subtle (number of interference fringes).

IV. PHASE DIAGRAMS

The above results are summarized in the universal phase-stability diagram (Fig. 9) where the lines of structural (Fréedericksz) transitions are plotted as functions of dimensionless parameters $\mu=R/d$ and d/ξ, measuring the relative anchoring strength and the relative external field strength, respectively. The transition lines are of first order (coexistence curves) and are plotted for two different ratios of elastic constants ($K_{33}/K_{11}=1$ and 2). Radial structures are stable at intermediate and strong anchoring strengths but weak external fields; axial structures are stable in weak fields only for weak anchoring strength, while they are stable for any anchoring strength in a strong external field. With an increased K_{33}/K_{11} ratio, the range of the stability of the radial structure and of the axial structure with a line defect increases, which is consistent with our discussion related to Fig. 7. At high anchoring strengths there is an intermediate region of field strengths where axial structures with a line defect are stable. In addition to transition lines, there are three interesting points: the zero-field radial-axial coexistence point $(\mu_0,0)$, the inversion point $(\mu_i,(d/\xi)_i)$, where the maximum transition field for the radial-axial transition is reached, and the triple point $(\mu_3,(d/\xi)_3)$, where all three phases coexist. The transition between the structures can be achieved either by varying the temperature or external field; varying the radius or other material-dependent parameters is possible by means of observing different systems. In our phase diagram the change of the field corresponds to a proportional displacement along the d/ξ axis, while a change in temperature corresponds to a nonproportional displacement in a general direction. This can be easily seen by taking into account that μ is proportional to $1/S(T)$ and d/ξ to $\sqrt{S}$ [see Eqs. (10) and (11)]. One can show that by changing the temperature, a transition between the axial and radial phase can be achieved but not a reentrance to the axial structure by crossing the radial stability area on the universal phase diagram [38].

In the region of large μ and d/ξ we have also analyzed the stability of the radial structure with the noncentral point defect. The results show that its free energy is

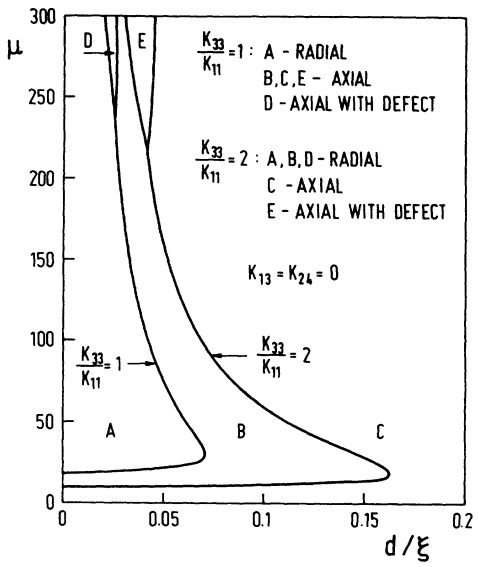

FIG. 9. Universal phase-stability diagrams of nematic droplets with homeotropic anchoring. Transition lines for two sets of bulk elastic constants are shown.

slightly above the free energy of the normal radial structure (difference $\sim 1\%$). But it might happen that a twisted structure becomes stable if $K_{22} < K_{11}, K_{33}$. This agrees with some polarization microscope observations [39,40]. The detailed treatment of the twist deformations requires a lot of computational time and will be published elsewhere.

Let us now include the K_{24} related surface contribution to the free energy and study the influence of this term on the stability regions of different droplet structures for the case $K_{ii} = K$ $(i = 1,2,3)$. The recalculation of the director fields shows that the effect on the three structures is significant only in the case of weak anchoring $(\mu < 20)$ and that it is limited to the region in the neighborhood of the droplet surface. The change of the orientation of the molecules at the droplet surface when taking into account the K_{24} elastic constant is illustrated in Fig. 10. Although the direct influence of the K_{24} contribution on the droplet structure is negligible, this term strongly influences the stability regions of different phases. The K_{24} surface term is comparable to remaining bulk terms in the expression for the free energy, but its contribution can be negative and thus favor the deformed structures. Its contribution is the largest in the radial structure, becomes smaller in the axial structure with line defect, and is smallest in the nonsingular axial structure. In the axial structure with the line defect the main surface contribution originates from the surface surrounding the isotropic core of the line defect, while such a contribution is negligible for the point defect of the radial structure. The stability region (see Fig. 11) of the radial structure increases relative to both axial structures, and the stability region of the axial structure with the line defect is pushed towards a larger value of d/ξ. In the case $K_{24} = 2K_{11}$ the radial structure is stable for zero anchoring strength parameter $(\mu_0 = \mu_i = 0)$ if the field parameter satisfies the relation $d/\xi < (d/\xi)_i$. This means that in the case where there is no interaction with the surrounding media (zero anchoring strength $\mu = 0$), an axial homogeneous structure would have the same energy as the radial structure; this does not seem to be a very real situation.

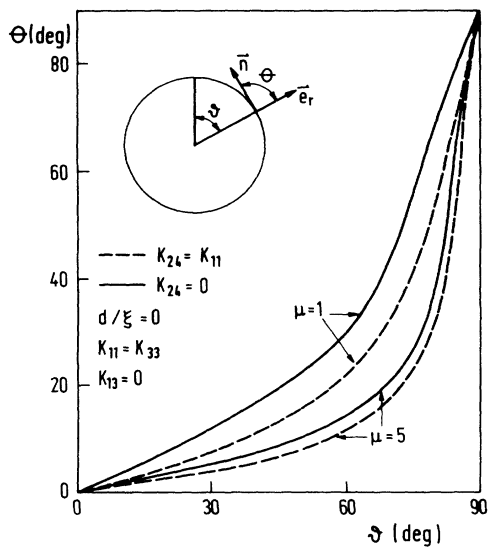

FIG. 10. Orientation of the director field on the droplet surface for different μ and K_{24} values.

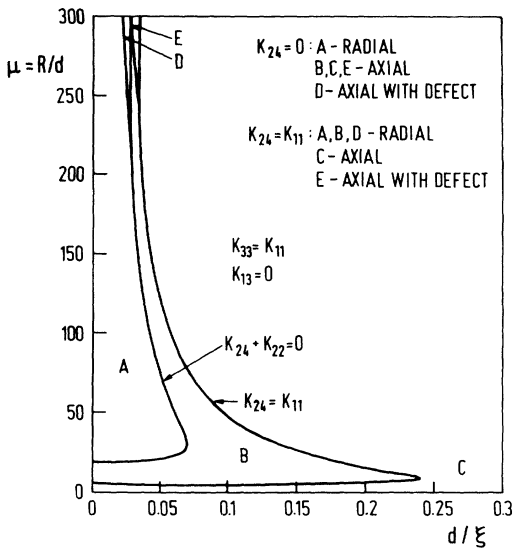

FIG. 11. Universal phase-stability diagrams of nematic droplets with homeotropic anchoring. Transition lines for two values of the saddle-splay elastic constants are shown.

The large effect of K_{24} on the stability diagram is expected to be useful in the experimental determination of the elastic constant K_{24}. Let us briefly discuss a possible way of determining the saddle-splay elastic constant and surface anchoring. Realizing that the product of the coordinates in our universal phase diagram $\mu d/\xi = R/\xi$ is independent of the anchoring strength W_0, we chose the inversion point and plot the value of $(R/\xi)_i$ as a function of K_{24} (Fig. 12). The value of $(R/\xi)_i$ is very sensitive to the value of K_{24} and could be used for its determination if $2 > K_{24}/K_{11} > 1$. Further examining the zero external field coexistence point $(\mu_0, 0)$ one finds that μ_0 strongly depends on K_{24} in the whole region of K_{24} values (Fig. 13). Knowing K_{24} would allow the determination of the anchoring strength $W_0 = (\mu K_{11}/R)_0$.

Our phase diagrams are consistent with recent experi-

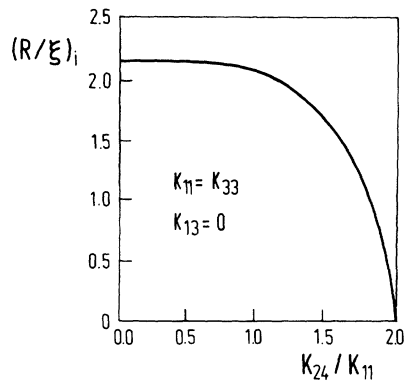

FIG. 12. Dependence of the inversion point ratio $(R/\xi)_i$ on the ratio of the elastic constants K_{24}/K_{11}.

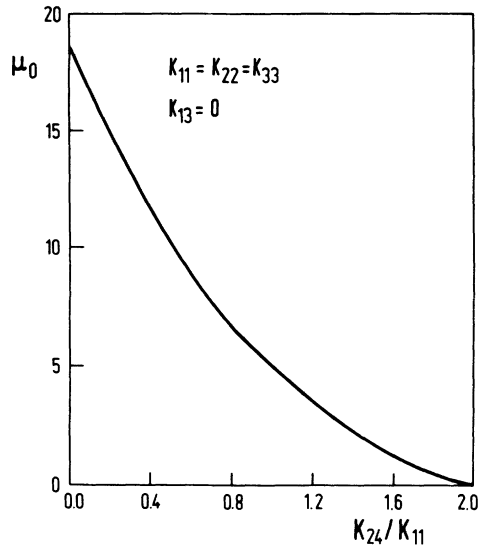

FIG. 13. Dependence of the zero field coexistence point (anchoring strength parameter μ_0) on the ratio K_{24}/K_{11}.

mental studies of PDLC materials performed with an optical polarized microscope in the external electric field [11], where the phase diagram was obtained in the weak anchoring limit, and neglecting the effect of K_{24}, the surface anchoring strength and the unknown internal electric field were estimated. As we have seen, the effect of K_{24} must be taken into account. This leads to three unknown quantities and enables the use of the above-mentioned experimental results for detailed comparison with theory or determination of K_{24} and W_0. The only conclusion besides the general agreement mentioned of the phase diagram shape is that because of the existence of the zero field axial phase, the inequality $K_{24}<2K_{11}$ must be true for the observed liquid-crystal material. This is consistent with preliminary estimates of K_{24} from NMR studies of nematic structures in cylindrical cavities [21,34].

V. CONCLUSIONS

In this paper we developed a phenomenological description of the stable nematic structures in supra-μm-size spherical droplets with homeotropic anchoring and constructed the field strength–anchoring strength phase diagram. The stability regions of structures with radial, nonsingular axial, and axial director field with a defect line are separated by first-order (Fréedericksz) transition lines. Particular attention is paid to three points: the zero field axial-radial coexistence point; the inversion point corresponding to the maximum external field where the radial structure is still stable; and the triple point where all three phases coexist. The importance of the saddle-splay elastic constant K_{24} for the stable regions of different structures is proven. In addition it is shown how this elastic constant could be measured by studying phase transitions in spherical droplets. A detailed discussion of the saddle-splay elastic constant determination including more subtle direct effects of K_{24} on structures, related microscope textures, and NMR spectra will be published elsewhere [38]. The experimental field-induced transition studies should be carried out in the magnetic field instead of the electric field where problems of internal field determination arise. Further studies are planned on the effect of twist K_{22} and splay-bend K_{13} elastic constants on structure. A detailed treatment of the defect in the direction field using a nonsingular biaxial core instead of an isotropic core approximation is expected to be important only for line defects. To show that in the case of point defects in supra-μm droplets one can neglect the details of the core structure, we used the model of Penzenstadler and Trebin [41] for the nonsingular biaxial core of a radial structure and compared its free energy to the free energy of the singular uniaxial director field. We estimate that replacing the uniaxial field with the biaxial one would lower the free energy only for about 0.1%, which is far below the estimated numerical error.

ACKNOWLEDGMENTS

One of the authors (S.Ž.) acknowledges the support of NSF Science and Technology Center Grant No. ALCOM DMR89-20147 while on visit at Kent State University.

APPENDIX

To obtain the set of differential equations for the director field corresponding to the case of a finite anchoring strength at the nematic-polymer interface, we start with the Landau–de Gennes free-energy density [see Eq. (9)] for uniaxial nematic ordering. We take into account that $\mathbf{n}$ is a unit vector by creating $f_{\text{Lagrange}}(\mathbf{r})$, which in addition to the free-energy density, includes surface $-\lambda_s(\mathbf{r})$ and volume $-\lambda_v(\mathbf{r})$ Lagrange multiplier fields:

$$f_{\text{Lagrange}}(\mathbf{r})=f(\mathbf{r})+\frac{\lambda_s}{2}\mathbf{n}\cdot\mathbf{n}\delta(\mathbf{r}-\mathbf{R})+\frac{\lambda_v}{2}\mathbf{n}\cdot\mathbf{n}\ . \tag{A1}$$

Minimizing the volume integral of the above expression with respect to $\mathbf{n}(\mathbf{r})$, the corresponding bulk and surface Euler-Lagrange equilibrium equation follows:

$$\frac{\partial f_e}{\partial n_i}+\frac{\partial f_f}{\partial n_i}-\left[\frac{\partial f_e}{\partial n_{i,j}}\right]_j+\lambda_v n_i=0\ , \tag{A2}$$

$$(\mathbf{e}_r)\frac{\partial f_e}{j\partial n_{i,j}}+\lambda_s n_i-W_0\mathbf{n}\cdot\mathbf{e}_r(\mathbf{e}_r)_i=0\ , \tag{A3}$$

where $\mathbf{e}_r$ stands for the surface normal unit vector. The second index stands for the derivative along the corre-

sponding coordinate and the repetition of the index in a term implies summation. The first equation is well known; therefore we are going to concentrate our attention on the second one. To eliminate the surface Lagrange field λ_s, we project Eq. (A3) on vectors $\mathbf{n}$ and $\mathbf{e}_r$ and combine the resulting equations. Finally using the notation introduced in Sec. III, the surface [Eq. (A3)] can be written as

$$k_{33}(\mathbf{e}_r,\mathbf{n},\nabla\times\mathbf{n})(\mathbf{n}\cdot\mathbf{e}_r)+[(\mathbf{n}\cdot\mathbf{e}_r)^2-1][(\nabla\cdot\mathbf{n})-\mu(\mathbf{n}\cdot\mathbf{e}_r)]$$
$$+k_{24}\{(\mathbf{n}\cdot\mathbf{e}_r)[\mathbf{e}_r(\nabla\mathbf{n})\mathbf{n}]-\mathbf{e}_r(\nabla\mathbf{n})\mathbf{e}_r$$
$$+(\nabla\cdot\mathbf{n})[1-(\mathbf{n}\cdot\mathbf{e}_r)^2]\}=0\ . \quad \text{(A4)}$$

As above, $K_{13}=0$ is assumed.

[1] J. W. Doane, N. A. Vaz, B. G. Wu, and S. Žumer, Appl. Phys. Lett. **48**, 269 (1986).
[2] J. Fergason, SID (Society for Information Display), Int. Symp. Digest Techn. Papers **16**, 68 (1985).
[3] J. W. Doane, A. Golemme, J. L. West, J. B. Whitehead, and B. G. Wu, Mol. Cryst. Liq. Cryst. **165**, 511 (1988).
[4] J. W. Doane, Mater. Res. Bull. **XVI**, 22 (1991).
[5] P. Sheng, Phys. Rev. A **3**, 1610 (1982).
[6] S. Kralj, S. Žumer, and P. W. Allender, Phys. Rev. A **34**, 2943 (1991).
[7] Dubois-Violet and O. Parodi, J. Phys. (Paris) **30**, C4-57 (1969).
[8] S. Candau, P. LeRoy, and F. Debeauvais, Mol. Cryst. Liq. Cryst. **23**, 283 (1973).
[9] G. E. Volovik and O. D. Lavrentovich, Zh. Eksp. Teor. Fiz. **85**, 1997 (1983) [Sov. Phys. JETP **58**, 1159 (1984)].
[10] P. Drzaic, Mol. Cryst. Liq. Cryst. **154**, 289 (1988).
[11] J. H. Erdmann, S. Žumer, and J. W. Doane, Phys. Rev. Lett. **64**, 19 (1990).
[12] M. J. Press and A. S. Arrott, J. Phys. (Paris) **36**, C1-177 (1975).
[13] R. D. Williams, J. Phys. A **19**, 3211 (1986).
[14] J. Bezic and S. Žumer, Liq. Cryst. (to be published).
[15] S. Žumer and J. W. Doane, Phys. Rev. **34**, 3373 (1986).
[16] J. W. Doane, S. Žumer, and A. Golemme, in *Proceedings of the Tenth Ampere Summer School and Symposium, Portorož, 1988,* edited by R. Blinc, M. Vilfan, and J. Slak (J. Stefan Institute, Ljubljana, 1988), p. 189.
[17] A. Golemme, S. Žumer, D. W. Allender, and J. W. Doane, Phys. Rev. Lett. **61**, 2937 (1988).
[18] A. Golemme, S. Žumer, J. W. Doane, and M. E. Neubert, Phys. Rev. A **37**, 559 (1988).
[19] E. B. Priestley, P. J. Wojtowitz, and P. Sheng, *Introduction to Liquid Crystals* (Plenum, New York, 1974), p. 143.
[20] F. C. Frank, Discuss. Faraday Soc. **25**, 19 (1958).
[21] D. W. Allender, G. P. Crawford, and J. W. Doane, Phys. Rev. Lett. **67**, 1442 (1991).
[22] A. Poniewierski and T. J. Sluckin, Mol. Phys. **55**, 1113 (1985).
[23] D. Monselesan and H. R. Trebin, Phys. Status Solidi B **155**, 349 (1989).
[24] G. Vertogen and W. H. de Jeu, *Thermotropic Liquid Crystals* (Springer-Verlag, Berlin, 1988).
[25] A. K. Sen and D. E. Sullivan, Phys. Rev. A **35**, 1391 (1987).
[26] H. Yokoyama, S. Kobayashi, and H. Kamei, J. Appl. Phys. **61**, 4501 (1987).
[27] W. J. A. Gossens, Mol. Cryst. Liq. Cryst. **124**, 305 (1985).
[28] P. G. de Gennes, *The Physics of Liquid Crystals* (Clarendon, Oxford, 1974).
[29] Guo-Ping Chen, Hideo Takezoe, and Atsuo Fukuda, Liq. Cryst. **5**, 341 (1989).
[30] G. Barbero and A. Strigazzi, Liq. Cryst. **5**, 693 (1989).
[31] A. Strigazzi, Mol. Cryst. Liq. Cryst. **152**, 435 (1987).
[32] V. H. Schmidt, Phys. Rev. Lett. **64**, 535 (1990).
[33] S. Žumer, S. Kralj, and J. Bezic, Proceedings of the European Conference on Liquid Crystals, Courmayer, 1991 [Mol. Cryst. Liq. Cryst. (to be published)].
[34] G. P. Crawford, D. W. Allender, J. W. Doane, M. Vilfan, and I. Vilfan, Phys. Rev. A **44**, 2570 (1991).
[35] J. Nehring and A. Saupe, J. Chem. Phys. **54**, 337 (1971); **56**, 5527 (1972).
[36] A. Saupe, J. Chem. Phys. **75**, 5118 (1981).
[37] R. Ondris-Crawford, E. P. Boyko, B. G. Wagner, J. Erdmann, S. Žumer, and J. W. Doane, J. Appl. Phys. **69**, 6380 (1991).
[38] S. Žumer and S. Kralj (unpublished).
[39] N. M. Golovataya, M. V. Kurik, and O. D. Lavrentovic, Liq. Cryst. **7**, 287 (1990).
[40] R. Ondris-Crawford (private communication).
[41] E. Penzenstadler and H. R. Trebin, J. Phys. (Paris) **50**, 1027 (1989).

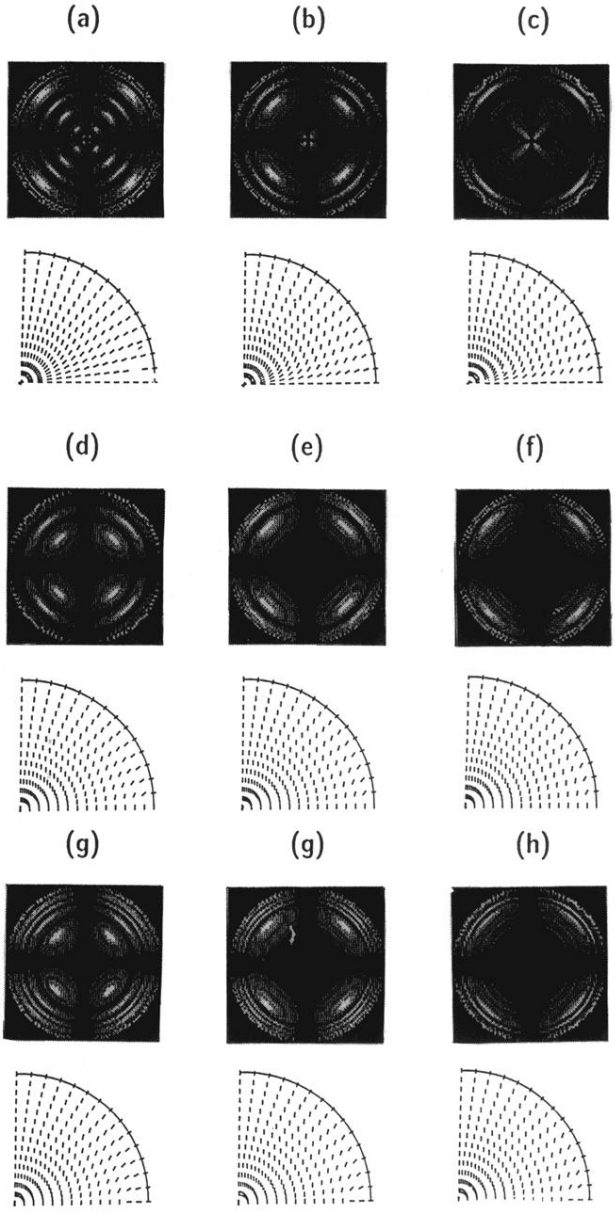

FIG. 8. Simulated monochromatic light polarization microscope textures and the corresponding director fields for different values of the field strength parameter d/ξ at $\mu=250$: (a) radial, $d/\xi=0.02$; (b) radial, $d/\xi=0.04$; (c) radial, $d/\xi=0.06$; (d) axial, $d/\xi=0.02$; (e) axial, $d/\xi=0.04$; (f) axial, $d/\xi=0.06$; (g) axial with defect, $d/\xi=0.02$; (h) axial with defect, $d/\xi=0.04$; (i) axial with defect, $d/\xi=0.06$. Simulation [37] was performed for $R/\lambda=28$ and with the extraordinary index of refraction $n_{\parallel}=1.7$ and the ordinary index of refraction $n_{\perp}=1.5$.